SNOWBALL EARTH

Rapid sea level rise in the aftermath of a Neoproterozoic snowball Earth

P. M. Myrow,[1]* M. P. Lamb,[2] R. C. Ewing[3]

Earth's most severe climate changes occurred during global-scale "snowball Earth" glaciations, which profoundly altered the planet's atmosphere, oceans, and biosphere. Extreme rates of glacioeustatic sea level rise are predicted by the snowball Earth hypothesis, but supporting geologic evidence has been lacking. We use paleohydraulic analysis of wave ripples and tidal laminae in the Elatina Formation, Australia—deposited after the Marinoan glaciation ~635 million years ago—to show that water depths of 9 to 16 meters remained nearly constant for ~100 years throughout 27 meters of sediment accumulation. This accumulation rate was too great to have been accommodated by subsidence and instead indicates an extraordinarily rapid rate of sea level rise (0.2 to 0.27 meters per year). Our results substantiate a fundamental prediction of snowball Earth models of rapid deglaciation during the early transition to a supergreenhouse climate.

Close monitoring of the Antarctic ice sheet indicates rapid and considerable collapse (1) due in part to anthropogenically induced climate change. Present rates of ice sheet collapse are constrained by observations, but little is known about rates during ancient deglaciations. The Late Neoproterozoic snowball Earth events represent an extreme climate change scenario, in which the collapse of global ice sheets during deglaciation is thought to have caused extremely large and rapid sea level rise (2–4). Complete deglaciation occurring over only 2000 to 10,000 years and rapid sea level rise are inferred from estimates of ice volume and greenhouse conditions (5), with CO_2 concentrations of ~400 to 660 times present-day atmospheric levels and surface temperatures of ~50ºC (2). However, paleomagnetic reversals within cap carbonate beds, which mantle glaciogenic deposits and are part of the glacioeustatic sea level rise succession (Fig. 1A), indicate slow deposition over >10^4 to 10^6 years (6, 7), presenting a major challenge to

the snowball Earth hypothesis. Such slow rise rates may be tied to late-stage thermal expansion of the oceans. However, early-stage rapid sea level rise from ice melt (4) is predicted, and geologic evidence for this has been lacking. Here we show that a siltstone unit that rests below a cap carbonate records the extremely rapid initial sea level rise predicted by the snowball Earth hypothesis.

The Elatina Formation in South Australia contains a distinctive record of the Marinoan snowball Earth (~635 million years ago) that includes evidence for ice advance and subsequent deglaciation, including the early postglacial interval, given that it is directly overlain by the Nuccaleena cap carbonate (8) (Fig. 1A). Paleomagnetic data constrain deposition of the formation to <15°N (9), supporting a low-latitude glaciation consistent with a snowball Earth. Within the deglaciation succession, a ~30-m-thick tidal-rhythmite siltstone unit records a complete daily record of sedimentation driven by tidal currents and wave action (10). We use a suite of sedimentary structures in

these deposits to test a fundamental prediction of the snowball Earth model—namely, rapid glacioeustatic sea level rise during deglaciation.

Siltstone of the upper Elatina Formation crops out across ~4500 km^2 of the Adelaide Rift Complex and Stuart Shelf of South Australia. It consists of centimeter-scale packages of ~12 pairs of millimeter-thick silt and muddy silt laminae [average grain sizes are 61 and 37 μm, respectively (11)] that vertically thicken and thin. These lamina pairs were initially considered to be varves formed in a periglacial lake (12) and later to be tidal delta deposits formed by spring-neap cycles (13). The rhythmites are preserved within bedforms (ripples) that aggrade vertically with few erosional surfaces, and individual bedforms can be continuously tracked vertically across meters of strata (8). Within this facies, several hierarchies of bedforms are preserved.

The first-order bedforms (i.e., the largest class) are straight-crested, relatively symmetrical ripples (Fig. 1, B and C) with average heights of $h = 1.8 \pm 0.6$ cm and average crest-to-crest spacings of $\lambda = 33 \pm 11$ cm ($\pm 1\sigma$) (table S1). Locally, cross-lamination is convex-up (Fig. 2A), typical of combined-flow ripples (14), and shows gradual vertical shifts, including reversals, in migration direction (Fig. 2C). Several new observations provide independent evidence that the large ripples were deposited under reversing tidal currents. First, the large ripple strata locally contain reactivation surfaces, which indicate a current reversal that eroded the bedform flank. Second, ripple–cross-laminated beds contain isolated, fully preserved ripples, less than 5 mm in height, that rest just below, or on, the larger ripple crests (Fig. 2B). These small ripples are oriented

[1]Department of Geology, Colorado College, Colorado Springs, CO 80903, USA. [2]Division of Geological and Planetary Sciences, California Institute of Technology, Pasadena, CA 91124, USA. [3]Department of Geology and Geophysics, Texas A&M University, College Station, TX 77843, USA.
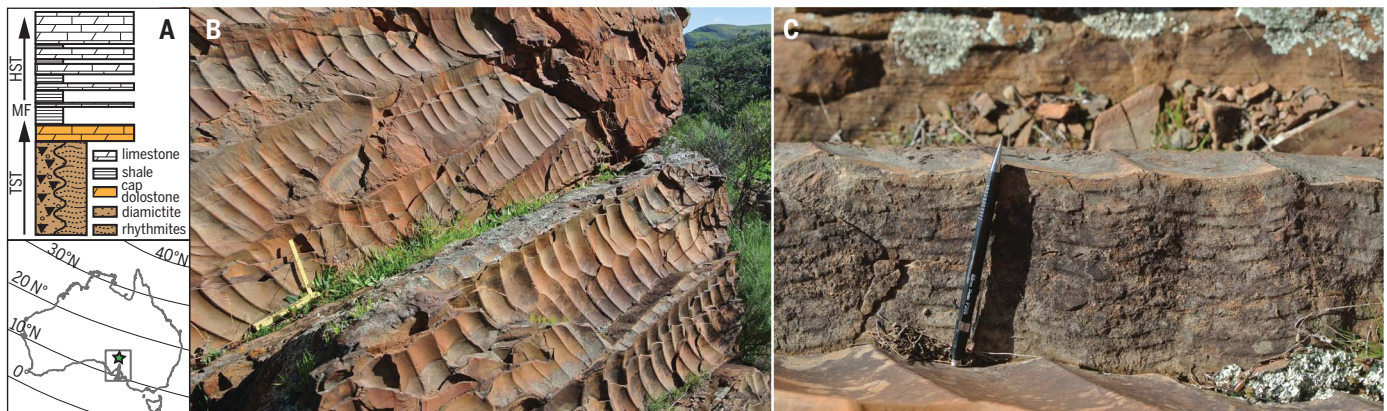*Corresponding author. Email: pmyrow@coloradocollege.edu

Fig. 1. Elatina Formation. (**A**) Generalized stratigraphic succession of Marinoan glacial and postglacial deposits [modified from (2)] and study location (star) with paleolatitude lines (26) in South Australia. TST, transgressive systems tract; MF, maximum flooding surface; HST, highstand systems tract. Black triangles indicate large clasts in diamictite. (**B**) Planview (bedding plane) outcrop showing larger first-order ripples oriented perpendicular to smaller second-order ripples with locally developed bifurcations. (**C**) Vertically climbing secondary ripples in cross section. Millimeter-scale tidal laminae are present. Laminae bundle boundaries are highlighted by centimeter-scale–spaced darker laminae. The pencil is 14 cm long.
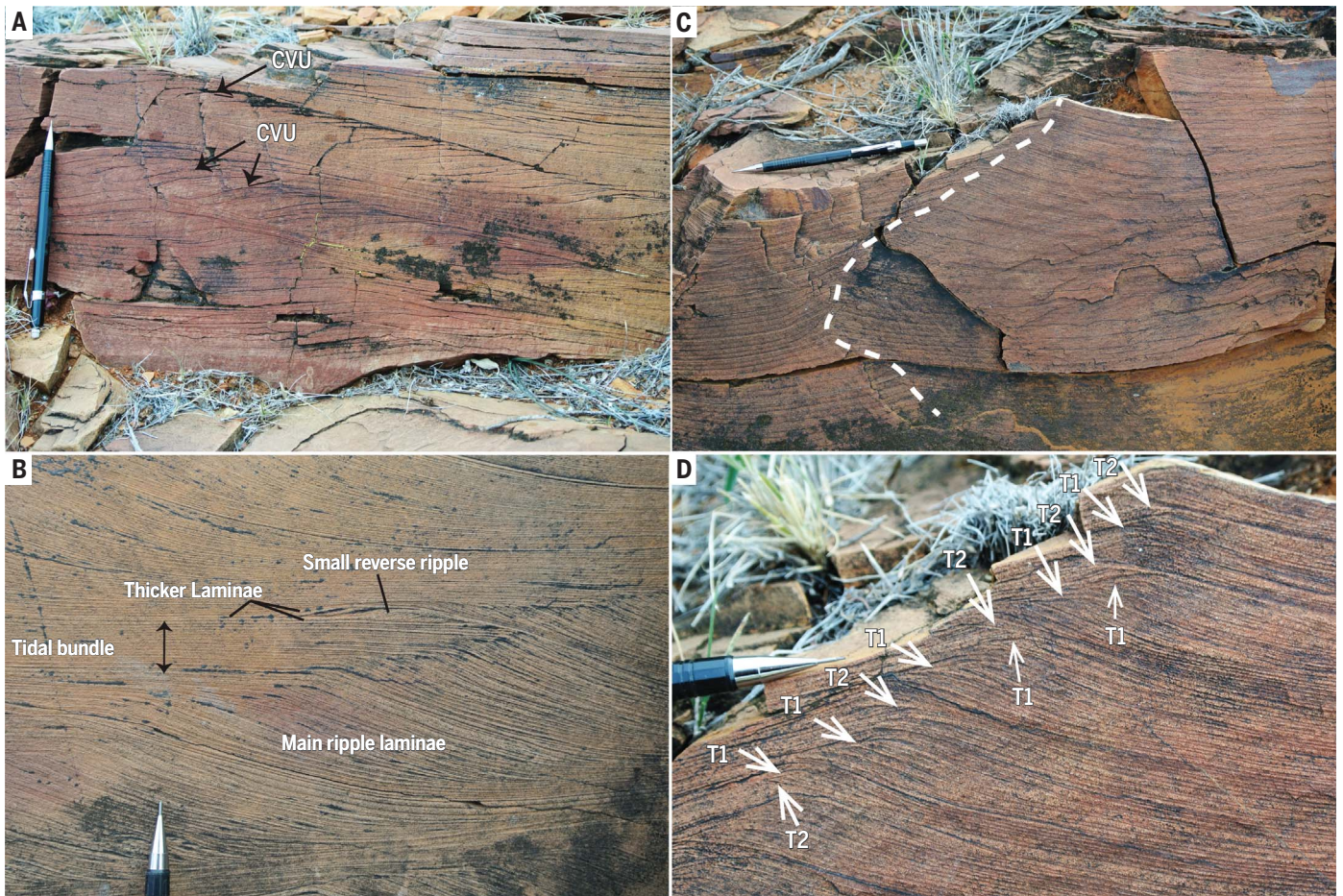
Fig. 2. Sedimentary structures of first-order ripples. (**A**) Stoss-erosional to nearly stoss-preservational first-order ripple cross-stratification with convex-up (CVU) lamination typical of combined-flow ripples. (**B**) Migrating ripple lamination with bundled tidal laminae. A small ripple with cross-stratification that dips opposite to the main ripple laminae is indicated. (**C**) Climbing first-order ripple cross-stratification, with the lower part recording bedform climb to the left and the upper part reversing to the right (the dashed line marks the position of the crestline over time), similar to cap carbonate strata (*27*). (**D**) Close-up of the upper part of (C). Surfaces that are moderately inclined to the left (T1) truncate the main cross-lamination of the ripple. Truncation surfaces that are flat to slightly inclined to the right (T2) become conformable downdip with laminae defining the cross-lamination of the ripple. These surfaces truncate laminae on the stoss side of the ripple that are dipping to the left. The two truncation-surface types generally alternate along the trace of the ripple crest. The pencil is 14 cm long.

opposite to the dominant ripple cross-lamination and are bounded by the thickest laminae of the tidal bundles, indicating that the strongest reversing currents (i.e., spring tides) produced traction transport against the dominant tide. Last, in cases, the first-order ripple cross-lamination contains two alternating types of erosional surfaces, half of which dip antithetical to the main cross-lamination and truncate the ripple foresets, whereas the other half dip in the dip direction of the large ripples, but at a lower angle (Fig. 2D). The two truncation-surface types alternate upward along the trace of the preserved climbing ripple crests, and the surfaces are contiguous with millimeter-thick white laminae that define rhythmite bundle boundaries, which again links the erosion surfaces to spring tides and cyclic lamination to reversing tidal currents.

The troughs of the first-order ripples preserve vertically aggraded second-order bedforms (i.e., smaller bedforms superimposed on the larger ones) that align perpendicular to the first-order ripple crests (Fig. 1B). The second-order bedforms consist of symmetrical to moderately asymmetrical two-dimensional ripples with $h = 0.4 \pm 0.2$ cm and $\lambda = 6.0 \pm 2.1$ cm (table S1). Second-order bedforms show locally developed bifurcations typical of straight-crested wave ripples. Their aspect ratio is $h/\lambda = 0.06 \pm 0.02$, and their ripple symmetry index, which is the ratio of the width of the stoss side to that of the lee side, is 1.9 ± 1.6 (table S2), making them consistent with postvortex anorbital wave ripples (*15*). Aspect ratios of these bedforms are smaller than those of wave ripples produced experimentally in sand but are consistent with ripples formed in silty sand beds in the presence of substantial suspension of mud (*16*).

The sedimentological characteristics indicate deposition during both wave and current activity in an ice-free body of water, consistent with the latest to post–snowball Earth climate. Whereas there is some spatial and stratigraphic variation, the most complete succession shows no systematic vertical changes in the heights and spacings of first- and second-order ripples throughout at least 16 m of the rhythmite unit (*8*). The small ripples are oriented north-northeast–south-southwest (fig. S1 and table S3), orthogonal to the first-order tidally influenced ripples, and thus the wave action that generated the second-order ripples was normal to the tidal currents, consistent with expected equatorial easterlies and northwest-oriented wind fields inferred from eolian dunes (*17*).

Wave ripples in sand and silt, whether orbital or anorbital, show a consistent relation between their aspect ratio, h/λ, and the formative wave orbital diameter, d_o (Fig. 3A), which can be used to reconstruct the paleo–water depth. For the Elatina wave ripples, we estimate $d_o = 0.95 \pm 0.15$ m (*11*). Wave generation constraints (*11*) dictate that for a given average wind speed and
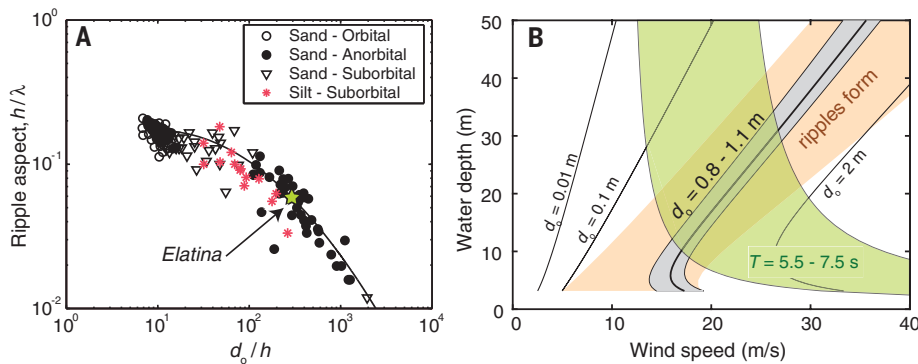
Fig. 3. Paleohydraulic reconstructions. (**A**) Wave ripple geometry (h, ripple height; λ, ripple crest-to-crest spacing) as a function of normalized orbital diameter, d_o. Sand-bed field data (28) include orbital, suborbital, and anorbital ripples. Silt-bed experiments (16) produced ripples with geometries and grain sizes similar to those of Elatina ripples. The solid line represents eq. S1 (11). (**B**) Combinations of average wind speed and water depth capable of producing $d_o = 0.95 \pm 0.15$ m (gray shading) according to a wave generation model (11). The orange-shaded region marks where wave ripples are stable (29) for 50-μm silt (11), and the green-shaded region corresponds to wave periods (T) of 5.5 to 7.5 s, conditions in which ripples similar to those of the Elatina formed in experiments (16). The reconstruction is based on a 75-km fetch inferred from paleogeographic reconstructions (10); varying fetch within a factor of 2 (38 to 150 km) has a negligible effect on the water depth.

$d_o = 0.95 \pm 0.15$ m, water depths varied by less than ~7 m (Fig. 3B). A near-uniform average daily wind speed is expected owing to trade winds, possibly modulated by diurnal katabatic winds (8). A larger change in water depth during deposition requires an unlikely systematic co-variation between depth and wind speed (Fig. 3B), and therefore relative sea level must have risen nearly commensurately with sediment accumulation.

Constraints on absolute water depth require an estimate of the wave period or average wind speed during ripple formation. Oscillatory duct experiments (16) with $d_o = 0.8$ to 1.0 m in silty sand produced ripples of equivalent dimensions to those in the Elatina Formation, with wave periods of $T = 5.5$ to 7.5 s. The wave generation model (11) indicates that this combination of wave parameters ($T = 5.5$ to 7.5 s and $d_o = 0.8$ to 1.1 m) limits absolute water depths to 9 to 30 m (Fig. 3B and fig. S2). The deeper end-member (30 m) requires the unlikely case of reoccurring whole gale–force winds (25 m/s), whereas the lower bound (9 to 16 m) indicates reasonable average wind speeds of ~16 m/s, equivalent to speeds previously proposed (8). Burial of the Elatina Formation would have been to ~5 to 6 km depth (18) with ~40% compaction (19). Thus, the original (decompacted) deposit thickness of ~27 m (11) exceeds our estimated maximum change in water depth (~7 m), in addition to the likely absolute water depth (9 to 16 m; Fig. 3B); these two independent constraints establish that the rate of relative sea level rise must have closely matched the accumulation rate.

The preservation of tidal laminae in the Elatina Formation provides a means to explain how two scales of superimposed bedforms accreted over 27 m with little change in ripple dimensions and inferred water depth. Williams (13) identified 1580 neap-spring tidal cycles in a 9.39-m-thick core of the Elatina Formation that was devoid of truncation surfaces, which he used to constrain depositional time, but he did not consider implications for sea level rise. Alternating thick and thin packages of laminae throughout the core, with each package containing ~12 pairs of silt and mud laminae, represent the neap-spring cycles within half a lunar month. Spectral analysis of these packages yielded the number of lunar months per year (13.1 ± 0.1) and a duration of 60.3 ± 0.5 years for the deposition of the 9.39-m-thick core (13). We use the resulting accumulation rate to estimate that the original thickness of ~27 m determined for our rippled section was deposited over ~100 years with an accumulation rate of ~27 cm/year (11), or 20 cm/year if water depth shallowed during deposition by the maximum amount allowed (7 m). This accumulation rate is higher than any previously estimated for a large marine basin over century time scales or longer (20) and is consistent with high suspended-sediment concentrations during rapid deglaciation of a snowball Earth episode. Given that subsidence over ~100 years would be negligible (21), the inferred ~27 m of accumulation could only be accomplished through a rapid rise in sea level, specifically at 20 to 27 cm/year.

The rhythmite unit represents a fraction of the total deglaciation deposit, and duration estimates for complete deglaciation, based on ice volumes and greenhouse conditions, are typically 2000 to 10,000 years (6000 years on average) (5). The total sea level rise due to melting of Marinoan glaciers has been estimated at ~1000 to 1500 m (2, 22), which likely varied spatially owing to gravitational effects (23). A glacioeustatic rise of 1.5 km over 2000 to 10,000 years corresponds to a long-term rise rate of 15 to 75 cm/year, or 25 cm/year for a 6000-year deglaciation, which is consistent with our independent short-term geologic constraint of 20 to 27 cm/year. This rate of sea level rise is 100 times as high as present-day rates (24) and five times as high as the highest rates during Pleistocene deglaciations (25). Sea level rise of this magnitude is a strong confirmation of a major tenet of the snowball Earth hypothesis—namely, rapid deglaciation during the early transition from icehouse to hypergreenhouse conditions.

REFERENCES AND NOTES

1. H. D. Pritchard et al., Nature **484**, 502–505 (2012).
2. P. F. Hoffman et al., Sci. Adv. **3**, e1600983 (2017).
3. J. L. Kirschvink, in The Proterozoic Biosphere, J. W. Schopf and C. Klein, Eds. (Cambridge Univ. Press, 1992), pp. 51–52.
4. J. Yang, M. F. Jansen, F. A. Macdonald, D. S. Abbot, Geology **45**, 615–618 (2017).
5. P. F. Hoffman, A. J. Kaufman, G. P. Halverson, D. P. Schrag, Science **281**, 1342–1346 (1998).
6. R. I. F. Trindade, E. Font, M. S. D'Agrella-Filho, A. C. R. Nogueira, C. Riccomini, Terra Nova **15**, 441–446 (2003).
7. B. Kilner, C. Mac Niocaill, M. Brasier, Geology **33**, 413–416 (2005).
8. C. V. Rose et al., Geosci. Can. **40**, 256–293 (2013).
9. D. A. D. Evans, T. D. Raub, Geol. Soc. London Memoirs **36**, 93–112 (2011).
10. W. V. Preiss, in The Adelaide Geosyncline: Late Proterozoic Stratigraphy, Sedimentation, Palaeontology and Tectonics, W. V. Preiss, Ed. (Bulletin 53, Geological Survey of South Australia, 1987), pp. 29–34.
11. Materials and methods are available as supplementary materials.
12. G. E. Williams, Nature **291**, 624–628 (1981).
13. G. E. Williams, J. Geol. Soc. London **146**, 97–111 (1989).
14. P. M. Myrow, W. Fischer, J. W. Goodge, J. Sediment. Res. **72**, 641–656 (2002).
15. H. E. Clifton, J. R. Dingler, in Wave-Dominated Coastal Environments, B. Greenwood, R. A. Davis Jr., Eds. (Elsevier, 1984), pp. 165–198.
16. M. P. Lamb, J. D. Parsons, J. Sediment. Res. **75**, 386–397 (2005).
17. G. E. Williams, Aust. J. Earth Sci. **45**, 733–741 (1998).
18. P. W. Schmidt, G. E. Williams, Earth Planet. Sci. Lett. **134**, 107–124 (1995).
19. J. P. Grotzinger et al., Science **350**, aac7575 (2015).
20. C. A. Partin, P. M. Sadler, Geology **44**, 1019–1022 (2016).
21. E. Carminati, G. Martinelli, Eng. Geol. **66**, 241–255 (2002).
22. P. F. Hoffman, Sedimentology **58**, 57–119 (2011).
23. J. R. Creveling, J. X. Mitrovica, Earth Planet. Sci. Lett. **399**, 74–85 (2014).
24. T. M. Cronin, Quat. Sci. Rev. **56**, 11–30 (2012).
25. T. Hanebuth, K. Stattegger, P. M. Grootes, Science **288**, 1033–1035 (2000).
26. R. C. Ewing et al., Earth Planet. Sci. Lett. **406**, 110–122 (2014).
27. P. A. Allen, P. F. Hoffman, Nature **433**, 123–127 (2005).
28. P. L. Wiberg, C. K. Harris, J. Geophys. Res. Oceans **99**, 775–789 (1994).
29. Z. J. You, B. Yin, Sedimentology **53**, 1181–1190 (2006).

Science

Rapid sea level rise in the aftermath of a Neoproterozoic snowball Earth

P. M. Myrow, M. P. Lamb and R. C. Ewing

A fast-melting snowball

The Marinoan "snowball Earth" glaciation covered most of the planet in ice. The surface melted only when enough carbon dioxide had accumulated in the atmosphere to trap the Sun's warmth. Melting must have occurred rapidly, but just how fast has been a topic of conjecture. Myrow *et al.* analyzed the wave ripples preserved in tidally deposited siltstones of the Elatina Formation, South Australia, to determine that sea level must have risen at the astounding rate of nearly 30 centimeters per year during the melting epoch, or roughly 100 times the rate that it is rising today.
Science, this issue p. 649

ARTICLE TOOLS	http://science.sciencemag.org/content/360/6389/649
SUPPLEMENTARY MATERIALS	http://science.sciencemag.org/content/suppl/2018/04/18/science.aap8612.DC1
REFERENCES	This article cites 29 articles, 10 of which you can access for free http://science.sciencemag.org/content/360/6389/649#BIBL
PERMISSIONS	http://www.sciencemag.org/help/reprints-and-permissions

Use of this article is subject to the Terms of Service